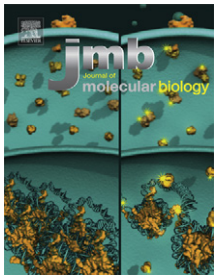

Molecular Basis for the Antiparasitic Activity of a Mercaptoacetamide Derivative That Inhibits Histone Deacetylase 8 (HDAC8) from the Human Pathogen *Schistosoma mansoni*

Diana A. Stolfa[1,†], Martin Marek[2,†], Julien Lancelot[3], Alexander-Thomas Hauser[1], Alexandra Walter[1,4,5], Emeline Leproult[2], Jelena Melesina[6], Tobias Rumpf[1], Jean-Marie Wurtz[2], Jean Cavarelli[2], Wolfgang Sippl[6], Raymond J. Pierce[3], Christophe Romier[2] and Manfred Jung[1]

1 - Institute of Pharmaceutical Sciences, *Albert-Ludwigs-Universität Freiburg, Albertstraße 25, 79104 Freiburg, Germany*
2 - Département de Biologie Structurale Intégrative, *Institut de Génétique et Biologie Moléculaire et Cellulaire, Université de Strasbourg, CNRS, INSERM, 1 rue Laurent Fries, BP 10142, 67404 Illkirch Cedex, France*
3 - Center for Infection and Immunity of Lille, *INSERM U1019–CNRS UMR 8204, Université Lille Nord de France, Institut Pasteur de Lille, 1 rue Professeur Calmette, F-59019 Lille Cedex, France*
4 - German Cancer Consortium (DKTK), *Freiburg, Germany*
5 - German Cancer Research Center (DKFZ), *Heidelberg, Germany*
6 - Institute of Pharmacy, *Martin-Luther-Universität Halle-Wittenberg, Wolfgang-Langenbeck-Straße 4, 06120 Halle/Saale, Germany*

Correspondence to Christophe Romier and Manfred Jung: *romier@igbmc.fr; manfred.jung@pharmazie.uni-freiburg.de*
http://dx.doi.org/10.1016/j.jmb.2014.03.007
Edited by S. Khorasanizadeh

Abstract

Schistosomiasis, caused by the parasitic flatworm *Schistosoma mansoni* and related species, is a tropical disease that affects over 200 million people worldwide. A new approach for targeting eukaryotic parasites is to tackle their dynamic epigenetic machinery that is necessary for the extensive phenotypic changes during the life cycle of the parasite. Recently, we identified *S. mansoni* histone deacetylase 8 (smHDAC8) as a potential target for antiparasitic therapy. Here, we present results on the investigations of a focused set of HDAC (*h*istone *d*e*ac*etylase) inhibitors on smHDAC8. Besides several active hydroxamates, we identified a thiol-based inhibitor that inhibited smHDAC8 activity in the micromolar range with unexpected selectivity over the human isotype, which has not been observed so far. The crystal structure of smHDAC8 complexed with the thiol derivative revealed that the inhibitor is accommodated in the catalytic pocket, where it interacts with both the catalytic zinc ion and the essential catalytic tyrosine (Y341) residue via its mercaptoacetamide warhead. To our knowledge, this is the first complex crystal structure of any HDAC inhibited by a mercaptoacetamide inhibitor, and therefore, this finding offers a rationale for further improvement. Finally, an ester prodrug of the thiol HDAC inhibitor exhibited antiparasitic activity on cultured schistosomes in a dose-dependent manner.

Introduction

The eukaryotic trematode *Schistosoma mansoni* is a human dioecious parasite that, together with other flatworms of the same genus (*Schistosoma japonicum*, *Schistosoma intercalatum*, *Schistosoma mekongi* and *Schistosoma haematobium*), causes the chronic tropical water-borne illness called schistosomiasis or bilharzia. According to World Health Organization statistics, over 230 million people in 77 endemic countries require treatment for schistosomiasis, which causes 280,000 deaths yearly, in sub-Saharan Africa alone [1]. Praziquantel is currently the only effective drug available for the treatment of schistosomiasis. However, its use is ineffective in case of recent infections [2], its application is limited to adult worms, it does not prevent reinfections and its mechanism of action still remains to be determined. Additionally, with large-scale control programs ongoing, there are worrying reports about the effectiveness of this drug being limited by increasing drug tolerance episodes [3,4]. It has already been reported in literature that the

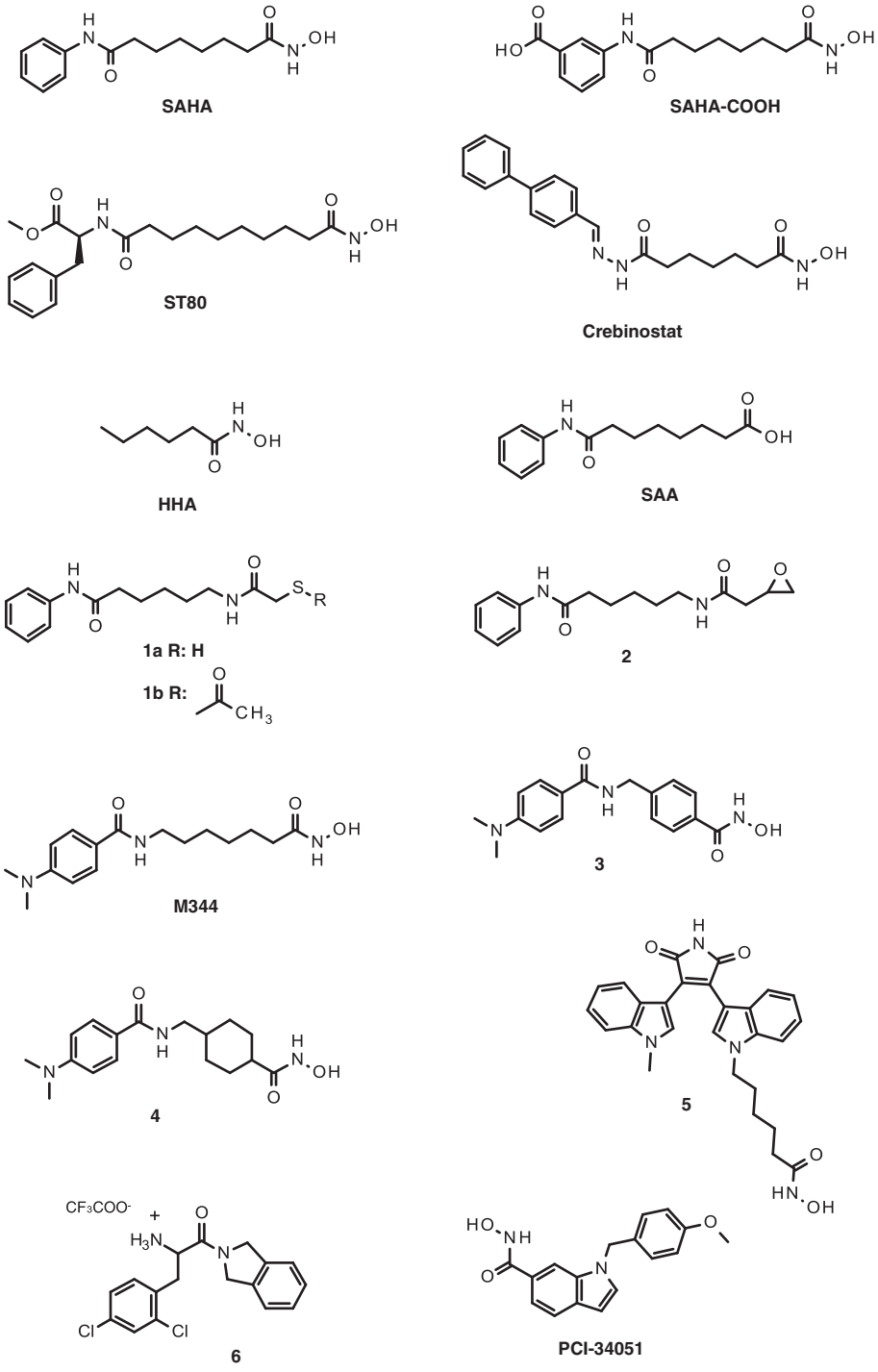

Fig. 1. Structures of HDAC inhibitors and test compounds.

expression of the efflux pump P-glycoprotein, often involved in drug resistance, is increased in schistosomes as a response to praziquantel exposure [5].

The large-sized genomes of three *Schistosoma* species have recently been characterized, proposing a correlation between the numerous phenotypic types that are crucial for its pathogenicity and the gene expression profiles during all its life cycle stages [6–9]. Epigenetic mechanisms play a central role in programed activation or silencing of gene expression and phenotype changes, by the means of an equilibrium of a large number of reversible post-translational

Table 1. *In vitro* inhibition results (IC_{50} values ± standard errors or percent inhibition at defined concentration) and ASP docking scores (higher scores suggest more favorable interactions) on smHDAC8 and hHDAC8

Inhibitor	Inhibition of smHDAC8	Inhibition of hHDAC8	ASP score smHDAC8	ASP score hHDAC8
SAHA	1.6 ± 0.2 μM	0.4 ± 0.1 μM	39.65	42.29
SAHA-COOH	1.9 ± 0.4 μM	0.4 ± 0.2 μM	33.36	37.38
ST80	0.8 ± 0.2 μM	0.3 ± 0.04 μM	38.58	46.67
Crebinostat	0.9 ± 0.3 μM	0.3 ± 0.02 μM	43.76	48.05
HHA	2.5 ± 0.4 μM	0.6 ± 0.1 μM	26.34	23.88
SAA	n.i. at 100 μM	n.i. at 100 μM	27.77	28.30
1a	50 ± 4 μM	200 ± 37 μM	27.71	26.96
2	n.i. at 100 μM	n.i. at 100 μM	34.15	29.92
M344	2.4 ± 2.0 μM	2.9 ± 1.5 μM	38.73	39.93
3	2.9 ± 0.3 μM	0.6 ± 0.04 μM	39.39	39.70
4	12 ± 2 μM	0.6 ± 0.1 μM	35.22	32.94
5	1.4 ± 0.2 μM	0.1 ± 0.02 μM	37.90	48.47
6	42.3% at 100 μM and 13.1% at 1 μM	1.1 ± 0.4 μM	28.11	25.83
PCI-34051	0.4 ± 0.1 μM	26 ± 8 nM	40.94	47.63

modifications that constitute the so-called "histone code" [10]. Modifications such as acetylation, methylation, phosphorylation, ubiquitinylation, SUMOylation or glycosylation on certain amino acid residues in histones or non-histone proteins are responsible for changes in the structure and stability of histone/histone and histone/DNA interactions, modulating gene expression and recruiting other proteins [11,12]. The balance of acetylation and deacetylation of histone lysine residues is catalyzed by histone acetyltransferases and HDACs (*h*istone *d*e*ac*etylases), respectively. The ε-amino residues of lysines in histone tails, when deacetylated, are able to compact the chromatin structure, usually resulting in a reduced accessibility of promoters for transcription factors and consequently inhibition of transcription [13,14]. This well-studied modification also occurs in *S. mansoni*, as previously described [15].

The family of zinc-dependent HDACs in human consists of 11 members that can be divided into three classes. In the parasite *S. mansoni*, three members of class I deacetylases are known, which represent orthologues of mammalian HDAC1, HDAC3 and HDAC8 [16]. HDAC8 from *S. mansoni* [*S. mansoni* histone deacetylase 8 (smHDAC8)] contains significant alterations of the catalytic domain as compared to orthologous enzymes of other organisms. While human HDAC8 (hHDAC8) shows the lowest level of expression of the four class I HDACs in human, in schistosomes, transcripts of smHDAC8 are expressed at higher levels than smHDAC3 and smHDAC1 during all life cycle stages, underlining its specific and vital functions in the parasite life cycle. All these peculiarities of smHDAC8 make it a promising target for the development of new species-selective drugs.

In previous work, we have validated smHDAC8 as a potential drug target and were able to solve its crystal structure, both in the apo-form and in complexes with different hydroxamate inhibitors [17]. In this latter study, the known HDAC inhibitors suberoylanilide hydroxamic acid (SAHA; Vorinostat) and M344 [18] (Fig. 1) were shown to inhibit smHDAC8 in the low-micromolar region that constituted the starting point for the work described in the present paper.

Results and Discussion

Focused library screening against smHDAC8

Here, in a focused library screening approach, we tested analogues of M344 and SAHA and representative HDAC inhibitors from in-house libraries and the literature for inhibition of smHDAC8. Generally, most HDAC inhibitors are represented by a general structure (see Fig. 1) that comprises a so-called warhead that usually complexes the zinc ion, a spacer that mimics the lysine methylene side chain and a so-called capping group that extends to the rim of the active-site tunnel. As analogues of SAHA, we used a newly synthesized carboxylic acid derivative (SAHA-COOH), the HDAC6-selective inhibitor ST80 [19], crebinostat [20] and hexanoylhydroxamate (HHA) that does not have an aromatic capping group. Additionally, we prepared three compounds that bear a variation of the warhead in SAHA. These are the carboxylic acid of SAHA (suberanilic acid, SAA [21]), a mercaptoacetamide analogue (**1a**) [22–25] and a newly synthesized epoxy ketone (**2**). The thiol **1a** and the epoxide **2** are simplifications of the well-known natural product inhibitors romidepsin [26,27] and trapoxin [28], respectively. For cellular testing of **1a**, we prepared the known thioester prodrug **1b** that liberates the active principle in cells [22,23]. As congeners of M344, we included a benzoic acid derivative (**3**) [18] and its 1,4-cyclohexylene analogue (**4**) [29]. As *S. mansoni* has also been shown to be susceptible to induction of apoptosis by sirtuin inhibitors [30], we also synthesized a new dual sirtuin/HDAC inhibitor (**5**) with a

Table 2. Data collection and refinement statistics

	smHDAC8/**1a**
Data collection	
Space group	*P*1
Cell dimensions	
a, *b*, *c* (Å)	70.8, 70.8, 98.0
α, β, γ (°)	77.8, 75.5, 85.4
Resolution (Å)	50.0–2.3
R_{sym}	0.106 (0.340)[a]
$I/\sigma(I)$	15.2 (4.2)
Completeness (%)	96.3 (93.8)
Redundancy	3.8 (3.8)
Refinement	
Resolution (Å)	32.0–2.3
No. of reflections	79,759
R-work/*R*-free	0.191/0.233
No. of atoms	
Protein	13,012
Ligands/ions	185
Water	451
B-factors (Å^2)	
Protein	26.5
Ligands/ions	39.6
Water	25.9
RMSD	
Bond lengths (Å)	0.01
Bond angles (°)	1.02
Ramachandran plot statistics (%)	
Favored	98
Allowed	2
Outliers	0

[a] Values in parentheses are for the highest-resolution shell (2.34–2.30 Å).

partial structure of the sirtuin inhibitor Ro 31-8220 [31]. As established inhibitors of hHDAC8, we selected a derivative of dichlorohomophenyl-*D*-alanine (**6**) [32] and **PCI-34051** [33]. We then tested the inhibition of smHDAC8 and hHDAC8 for all these compounds. We used a commercially available homogenous fluorescence assay [Fluor de Lys(R)-HDAC8] with an acetylated tetrapeptide sequence derived from p53 (Arg-His-AcLys-AcLys-Fluorophor) as substrate. The results are displayed in Table 1.

The results of the *in vitro* assays revealed that all inhibitors with a hydroxamic acid warhead are inhibitors of both the *S. mansoni* and the human enzyme in the low-micromolar range or even below with a slight selectivity for the human isoform over the schistosomial HDAC8. The nature of the capping group seems to be of little importance in our set, at least for affinity to the human enzyme. Even the simple alkyl derivative HHA is in the submicromolar range. For analogues of M344, increased steric bulk in the spacer (compounds **3** and **4**) decreased activity, whereas **PCI-34051** with an indole spacer is nevertheless in the submicromolar range. Obviously, in more rigid molecules, the relative position of hydroxamate and capping group is of great importance for affinity. Exchange of the hydroxamate warhead generally leads to a substantial loss of activity in smHDAC8 and, with the exception of **6**, also for hHDAC8. However, while the carboxylic acid SAA and the epoxy ketone **2** are completely inactive, the thiol **1a** retained activity specifically for smHDAC8 around 50 μM.

The smHDAC8 preparation that was used in the assays contains DTT, which is a well-known reducing agent able to break disulfide bonds. We also prepared a DTT-free preparation of smHDAC8 and tested the inhibition of the thiol inhibitor. Compound **1a** showed a reduced inhibition of smHDAC8 without DTT (157.8 ± 18.6 μM; data not shown), which suggests that the dithiol probably serves to prevent disulfide formation or further oxidation of the thiol inhibitor.

Crystal structure of smHDAC8 in complex with the mercaptoacetamide inhibitor 1a

To rationalize the inhibition of smHDAC8 by the mercaptoacetamide **1a**, we determined the crystal structure of smHDAC8 in complex with this compound. Crystallographic data of the complex at 2.3 Å resolution were collected. The refined model of this complex has low *R*-factors and shows good refinement statistics (Table 2). In general, no dramatic conformational changes were observed in smHDAC8 upon binding of **1a** when compared to the native smHDAC8 and inhibited forms of smHDAC8 structures described recently [17]. Most of the residues could be built in density, except for a few disordered loops. The mercaptoacetamide inhibitor binds to each monomer in the asymmetric unit of the crystal with full occupancy and its electron density was perfectly defined and unambiguously interpretable as shown in Fig. 2.

As noted above, **1a** is an HDAC inhibitor composed of a mercaptoacetamide warhead, a hydrophobic flexible linker domain and a hydrophobic capping group. The crystal structure of the smHDAC8/**1a** complex reveals that the inhibitor is accommodated in the catalytic pocket, where it interacts with both the catalytic zinc ion and Y341 via its mercaptoacetamide group (Figs. 2 and 3).

To our knowledge, after the hHDAC8/largazole complex structure [34], this is only the second structure of an HDAC complex, where a sulfur–Zn^{2+} coordination is observed and the first one for any mercaptoacetamide. The zinc ion coordination geometry in the smHDAC8/**1a** structure is tetrahedral and similar to that observed in the hHDAC8/largazole structure, with ligand–Zn^{2+}–ligand angles ranging from 100° to 119° (Fig. 3). The S–Zn^{2+} distance ranges between 2.2 and 2.3 Å across all monomers (A to D) in the asymmetric unit. The optimal tetrahedral zinc coordination likely provides a significant contribution to smHDAC8–**1a** affinity.

However, and in contrast to largazole, the mercaptoacetamide head of the inhibitor makes a further contact with an active-site residue, namely, the catalytic tyrosine Y341 (Fig. 2). Specifically, Y341 adopts the

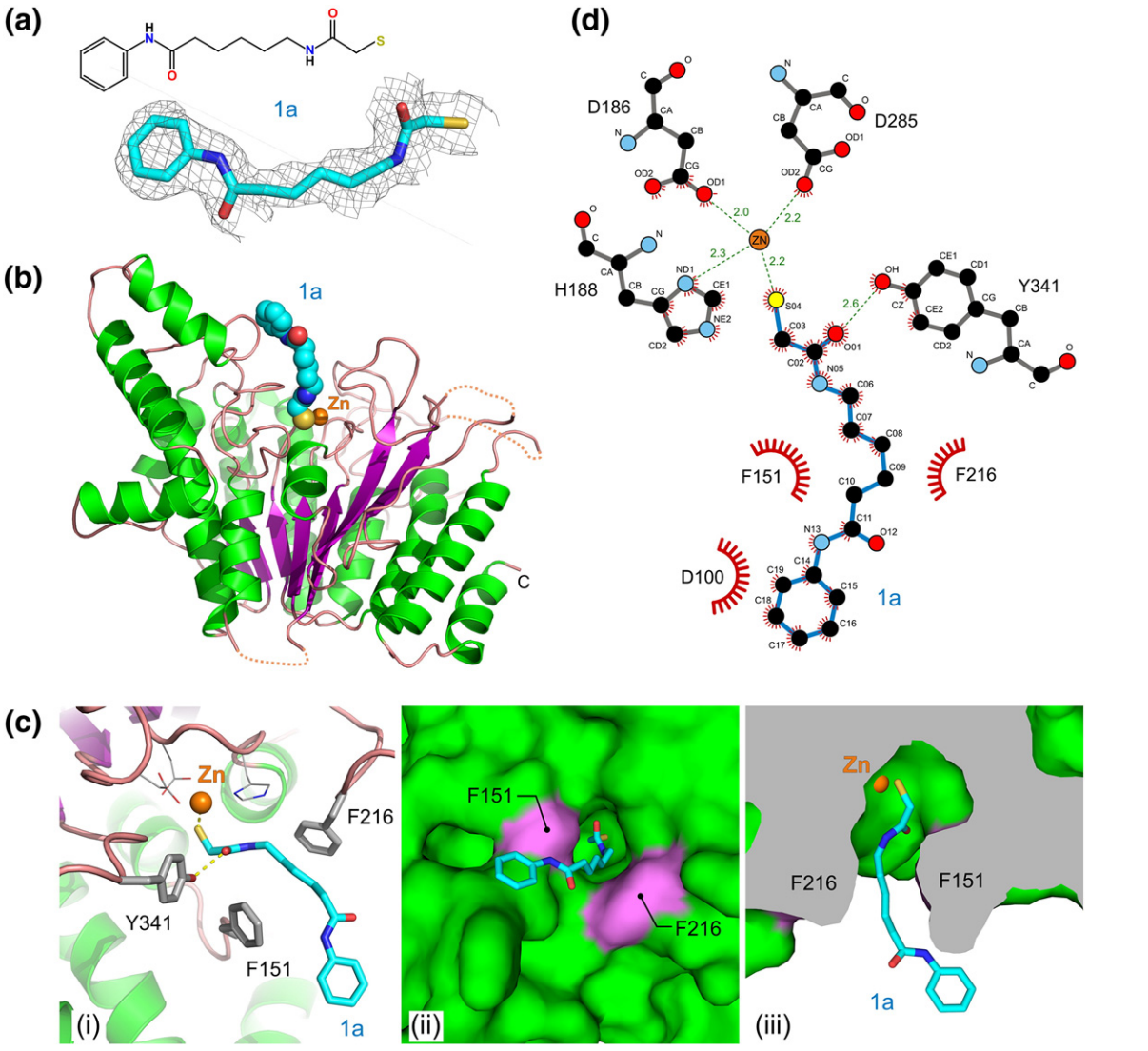

Fig. 2. Structural insight into the smHDAC8 inhibition by the mercaptoacetamide inhibitor **1a**.(a) Representation of **1a** and calculated simulated annealing omit map contoured at 1.2 σ around the inhibitor observed in the crystal structure of the smHDAC8/**1a** complex.(b) Ribbon diagram of the overall structure of smHDAC8 together with the catalytic zinc ion (orange sphere) and the bound inhibitor represented in space filling.(c) Close-up views of the active site of smHDAC8 (shown as sticks) with bound inhibitor **1a** shown as (i) ribbon, (ii) surface view and (iii) side cut-away surface view.(d) Schematic representation of the interactions formed by the mercaptoacetamide inhibitor with the smHDAC8 active-site zinc ion and residues.

flipped-in conformation, as seen in hydroxamate-inhibited smHDAC8 structures for example [17], that facilitates an interaction of its hydroxyl group with the carbonyl atom of the mercaptoacetamide group (Fig. 2). Interestingly, upon **1a** binding, smHDAC8 F151 fully occupies an unusual flipped-in conformation [17] and, together with F216, forms the hydrophobic tunnel that accommodates the slightly kinked aliphatic linker of the inhibitor. The measured C–C–S–Zn dihedral angle in the X-ray structure of largazole/HDAC8 is on average 92.4° (88.1 and 96.6 for monomer A and monomer B, respectively). For the thiol **1a**/smHDAC8 structure, we observed an average value of 12.9° (28.4, 26.8, −17.0 and 13.5 for the individual monomers). The difference in the dihedral angles can be explained by additional hydrogen bonds that are observed with the protein. In case of largazole, the thiol makes an additional hydrogen bond with Tyr306, whereas in case of **1a**, the carboxamide makes the hydrogen bond with Tyr341.

Thus, the binding of the mercaptoacetamide group to the catalytic zinc results in a different positioning of the hydrophobic linker and capping group that **1a** has in common with SAHA. However, both inhibitors bind quite differently into the smHDAC8 active site. This might explain why on one hand an increase in

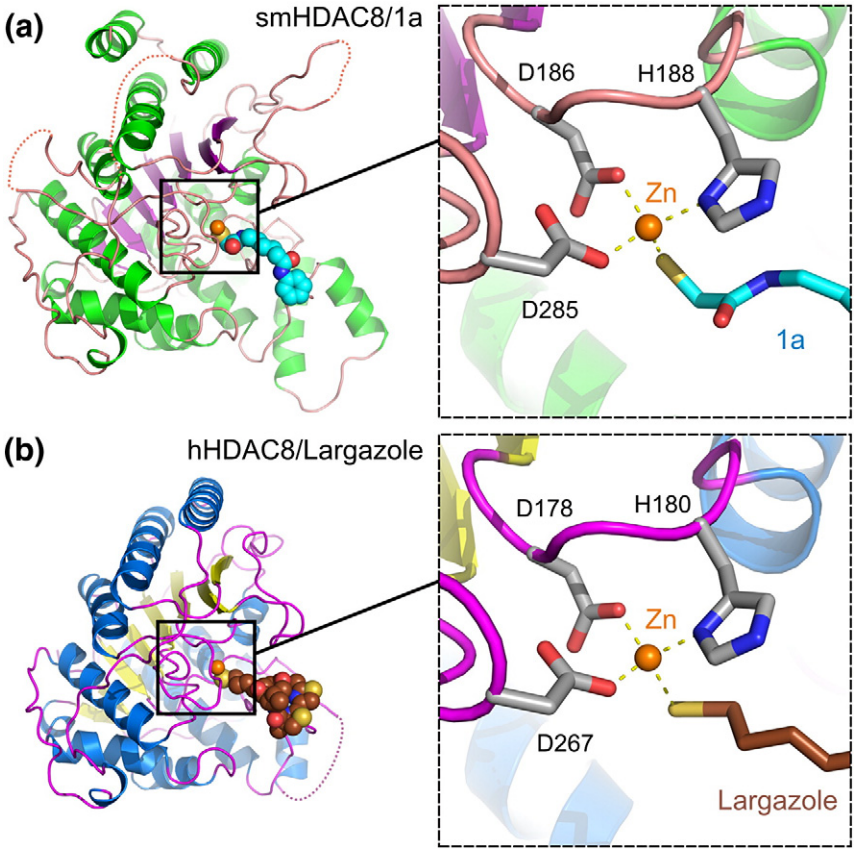

Fig. 3. Tetrahedral coordination of the zinc ion bound in the active site in smHDAC8/**1a** and hHDAC8/largazole complexes. (a) Overall structure of *S. mansoni* HDAC8 together with the catalytic zinc ion (orange sphere) and the bound inhibitor **1a** represented in space filling. The inset shows close-up view of the smHDAC8 active site. Residues involved in the zinc coordination are drawn with sticks. The carbon atoms of proteins side chains are in gray, whereas the carbon atoms of **1a** are in cyan. Yellow broken lines represent the coordination of the zinc ion by protein residues and the inhibitor.(b) Overall structure of hHDAC8 together with the catalytic zinc ion (orange sphere) and the bound largazole inhibitor represented in space filling. The inset shows close-up view of the hHDAC8 active site. Residues involved in the zinc coordination are drawn with sticks. The carbon atoms of proteins side chains are in gray, whereas the carbon atoms of **1a** are in brown. Yellow broken line represents the coordination of the zinc ion by protein residues and largazole.

the IC_{50} value of **1a** compared to SAHA is observed, but the selectivity is shifted toward the parasite enzyme. Further improvements of **1a** are necessary to increase the potency of inhibitors with a mercaptoacetamide warhead while maintaining its favorable selectivity as compared to SAHA.

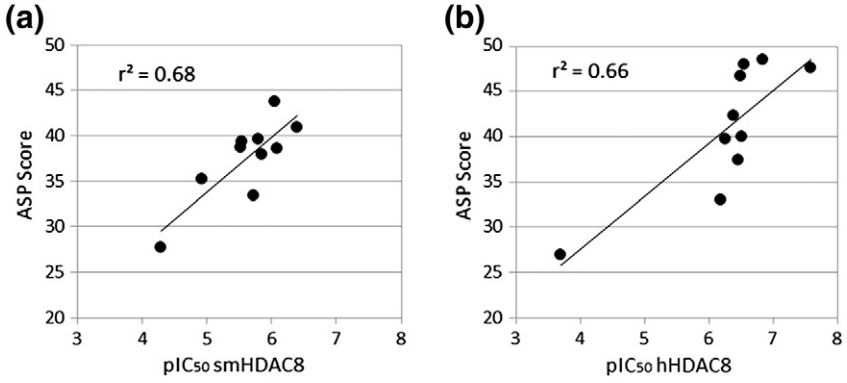

Fig. 4. Observed correlation between *in vitro* pIC_{50} values and calculated ASP docking scores for smHDAC8 (a) and hHDAC8 (b) computational models.

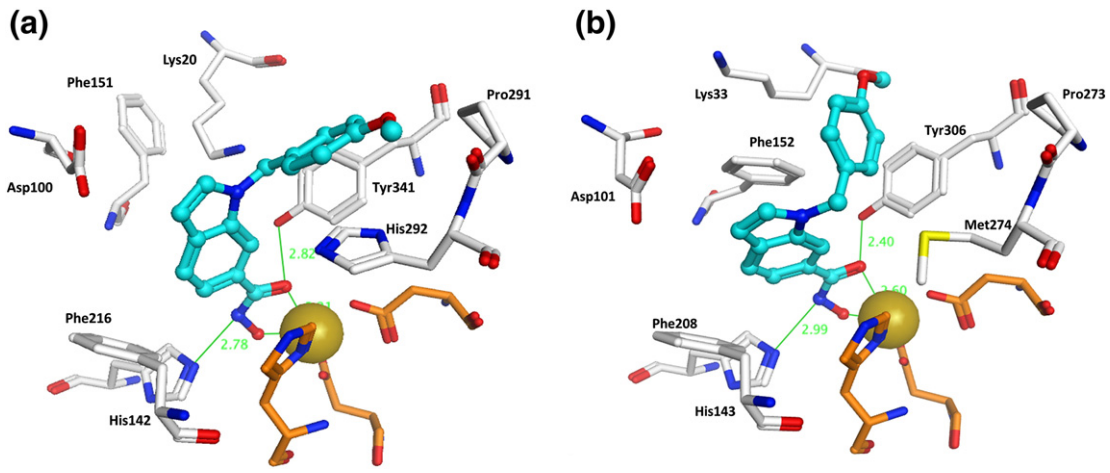

Fig. 5. Docking poses observed for the most active compound **PCI-34051** (colored cyan) at the smHDAC8 (a) and hHDAC8 binding pocket (b). Only interacting amino acids are displayed for clarity. Residues coordinating the zinc ion are colored orange and hydrogen bonds/coordination to the zinc ion is indicated by the green lines (distances are given in angstroms).

Docking studies and rationalization of structure–activity relationships

To predict the binding mode of the tested compounds and to rationalize the structure–activity relationships, we carried out a molecular docking study for *S. mansoni* and hHDAC8. For both enzymes, crystal structures that were used to find the right docking setup are available (see Experimental Procedures for details). Using this setup, we were able to reproduce the known crystal structures of *S. mansoni* HDAC8 in complex with SAHA resp. M344 and the thiol **1a** from this study (RMSD values below 1 Å). The results show that the docking and scoring models (using the ASP score) can be used to discriminate between active and inactive/weakly active compounds (Table 1), and in general, a correlation between the docking scores and pIC_{50} values was observed (Fig. 4). All inactive compounds and compounds active above 15 μM received docking scores below 29, except compound **2**. Active compounds, usually hydroxamates, received favorable docking scores above 32, except HHA and compound **6** in case of hHDAC8. All hydroxamates show coordination to Zn^{2+} with the hydroxamic acid group and fit nicely into the pocket of both smHDAC8 and hHDAC8. However, we also observed that the scoring functions (including ASP score) have problems for correctly ranking the non-hydroxamates.

Beside the problem of correctly scoring different zinc-binding groups, we suppose that the known protein flexibility of HDACs might be responsible for the incorrect ranking of some compounds (**2**, **6** and **HHA**). For example, in case of compound **6**, the conformational change of hHDAC8 upon binding of this ligand is observed in its X-ray structure (PDB ID: 3SFH) [30]. The dichlorophenyl group fits into the putative acetate release channel, which is opened mainly by the movement of the Trp141 side chain in hHDAC8. This conformational change is not possible in smHDAC8 due to the surrounding residues. The movement of Trp140 in smHDAC8 (corresponding to Trp141 in hHDAC8) might be prevented by Phe21, which corresponds to Ile34 in hHDAC8. Consequently, the α-amino-ketone group of **6** cannot reach Zn^{2+} inside the binding pocket, which explains the weak activity on smHDAC8.

The docking pose of **PCI-34051**, the most active compound tested on hHDAC8 and smHDAC8, shows that the hydroxamic acid coordinates Zn^{2+} and the aromatic indole interacts with several aromatic residues in both enzymes (Fig. 5). In complex with hHDAC8, the methoxyphenyl group is embedded in a hydrophobic pocket formed by Phe152, Pro273, Met274 and Tyr306. This pocket is more polar in smHDAC8 where Met274 is substituted to His292, which might explain the weaker enzymatic inhibition and the lower calculated scores. Also for the other active hydroxamates, such as crebinostat and ST80 for example, an interaction with this hydrophobic side pocket in both enzymes is observed (see Fig. S1a–d).

Antiparasitic activity

Because it is well known that, for cellular activity in sulfur-based HDAC inhibitors, thiol esters should be employed rather than the free thiols, the ester **1b** was tested for anti-schistosomal activity. The inhibitor **1b** decreases the viability of cultured schistosomula in a dose- and time-dependent manner in the range 10–50 μM (Fig. 6). Moreover, similar to pan-HDAC inhibitors [15], induction of apoptosis at 20 and 50 μM **1b** was shown using TUNEL (*t*erminal deoxynucleotide transferase d*U*TP *n*ick *e*nd *l*abeling) staining (Fig. 7).

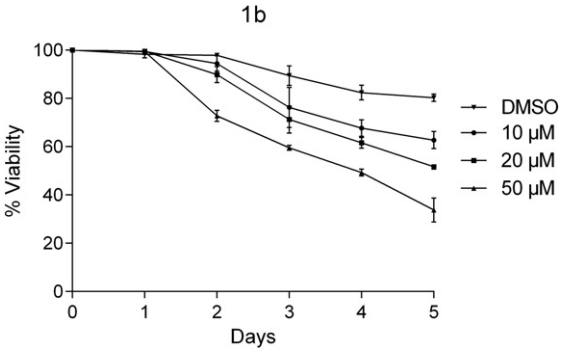

Fig. 6. Decrease in viability in cultured schistosomula treated for up to 5 days with increasing concentrations of **1b**. Dead and dying larvae are dark and opaque and present granular aspects and tegumental damage. Results are expressed as mean percentage of surviving larvae (±SEM, three independent experiments).

Conclusions

Among a small focused library of HDAC inhibitors that were tested for inhibition of *S. mansoni* HDAC8 as potential antiparasitic agents, a thiol analogue (**1a**) of the hydroxamate inhibitor SAHA showed decreased potency but increased selectivity for smHDAC8 over hHDAC8. The HDAC8 reference inhibitor **PCI-34051** shows potent activity against smHDAC8, suggesting indoles as an optimized spacer motif for affinity to the parasite enzyme. We were able to solve the structure of the thiol inhibitor bound to smHDAC8 as a first example of a co-complex of a mercaptoacetamide with an HDAC of any origin. Interestingly, just by exchange of the zinc-coordinating warhead, a completely different binding mode of **1a** as compared to SAHA is observed [17], although spacer and capping group are the same. This can be realized due to the flexibility of the spacer and the flexible nature of key phenylalanine residues that shape the acetyl lysine tunnel in smHDAC8. Additionally, we have shown antiparasitic activity of the thiol ester prodrug **1b** on cultured schistosomes.

smHDAC8 has been validated as a unique therapeutic target by transcript invalidation using RNA interference before, but we cannot rule out the possibility that the antiparasitic effect of inhibitor **1b**, at least in part, may have been due to the inhibition of other *Schistosoma* HDACs. In literature, usually hydroxamate warheads are given priority in studies on HDAC inhibitors but there is also continuing interest in sulfur-based warheads [35,36]. Especially interesting is the fact that, in a cellular model of neuroprotection, mercaptoacetamides were active while structurally similar hydroxamates were not [37]. Taken together, our results serve as a rational basis for the further structure-guided optimization of HDAC inhibitors for both potency and species selectivity as potential therapeutics against schistosomiasis.

Experimental Procedures

Chemistry and inhibitors

The inhibitors **PCI-34051** and SAHA were purchased from Selleck Chemicals; SAA, at Biozol; and HHA, at Chemical Book. Synthetic procedures and spectral characterization data are presented in detail in the supplemental material. All chemicals were purchased from Sigma, Aldrich or Fluka and used without further purification. Starting materials, reagents and analytical-grade solvents were obtained from commercial sources. T_3P 50% weight in THF and 50% weight in DMF were kindly donated by Archimica (Frankfurt, Germany). Chromatographic separations were performed on silica gel (15–40 mesh; Merck) using flash methodology. Reaction progress was monitored by analytical thin-layer chromatography on pre-coated silica gel (Kieselgel 60 F254) plates, and spots were detected by UV light (λ = 254 nm). Melting points of the final target HDAC inhibitors were determined by the open capillary method on a Stuart-Scientific SMP3 electrothermal apparatus and are uncorrected. ^{1}H NMR spectra were recorded in the indicated deuterated solvents on a BrukerAvance

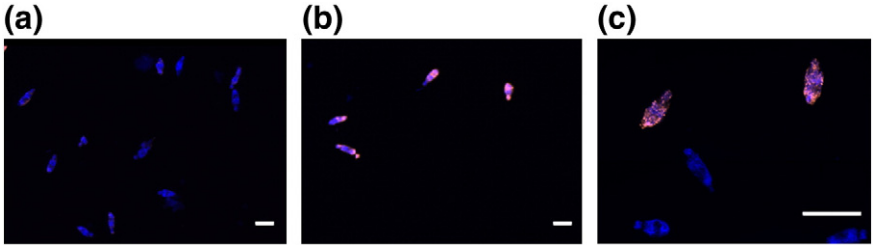

Fig. 7. TUNEL staining for apoptosis in cultured schistosomula induced by different concentrations of **1b**. (a) DMSO control, (b) 20 μM **1b** and (c) 50 μM **1b**. Background staining was performed using 4′,6-diamidino-2-phenylindole. Positively TUNEL labeled schistosomula are red. The intensity of labeling, as well as the number of positively stained larvae, increased with the dose of inhibitor used. Size bars in all three panels represent 100 μm.

DRX 400-MHz spectrometer, and ^{13}C NMR, on a Varian 100 MHz. Chemical shifts (δ) are expressed in parts per million, and coupling constants (*J*) are in hertz. The following abbreviations are used: bs (broad singlet), s (singlet), d (doublet), dd (double doublet), t (triplet), dt (double triplet), m (multiplet); signals due to OH and NH protons were located by deuterium exchange with D_2O. EI and CI mass spectra were measured with a TSQ700 mass spectrometer (Thermoelectron). ESI and PCI mass spectra were recorded with a LCQ-Advantage mass spectrometer. In all cases, spectroscopic data are in agreement with known compounds and assigned structures. HPLC purity determinations were performed on a JASCO HPLC system under isocratic conditions, using a PhenomenexSynergi Hydro RP-C18 column (250 mm × 4.6 mm, 4 μm particle size). Elution was performed using 0.05% of TFA in H_2O/ACN 60/40 (v/v), at room temperature. The purity of all tested compounds was ≥98%, as measured by HPLC. Injection volumes were 2 μL, flow rate was 0.5 mL/min and detection was performed with UV (λ = 254 nm).

In vitro HDAC inhibition assay, enzymes

The activity of compounds prepared for this study was evaluated using an HDAC enzyme inhibition homogenous fluorescence assay. The HDAC activity assay was performed using a commercial HDAC8 Fluorimetric Drug Discovery Kit [Fluor de Lys(R)-HDAC8, BML-KI178] according to the manufacturer's instructions. The enzyme was incubated for 90 min at 37 °C, with a substrate concentration of 50 μM and increasing concentrations of inhibitors. Fluorescence intensity was measured in a plate reader (BMG Polarstar) with excitation wavelength set at 390 nm and emission detection set at 460 nm.

The gene coding for the smHDAC8 protein was introduced into a pnEA/tH expression vector [38], and the smHDAC8 protein was produced according to the same protocol as described previously [17]. Briefly, overexpression was carried out in *Escherichia coli* BL21(DE3) cells in Terrific Broth medium. Induction was performed at 37 °C by adding 0.5 mM final isopropyl-1-thio-β-D-galactopyranoside (Euromedex), in the presence of 100 μM $ZnCl_2$. Harvested bacteria were resuspended in lysis buffer [50 mM KCl and 10 mM Tris–HCl (pH 8.0)] and lysed under high pressure (18,000 psi) in a Microfluidizer Processor M-110EH (Microfluidics). The lysate was clarified by ultracentrifugation (40,000 rpm; Ti45 Beckman) for 1 h. The supernatant was loaded onto Talon metal affinity resin (Clontech) pre-equilibrated with the lysis buffer. The His-tagged smHDAC8 protein was released from the Talon resin by thrombin treatment and subsequently loaded onto a 1-mL HiTrap Q FF (GE Healthcare) column pre-equilibrated with the lysis buffer. The protein was eluted by a linear gradient of KCl (50 mM to 1 M KCl) and then loaded onto HiLoad 16/60 Superdex 200 gel-filtration column (Amersham Bioscience) equilibrated in 50 mM KCl, 10 mM Tris–HCl (pH 8.0) and 2 mM DTT when required (see the text).

In vitro sirtuin inhibition, enzymes

Human Sirt1 (amino acids 133–747), human Sirt2 (amino acids 25–389) and human Sirt3 (amino acids 101–399) were recombinantly expressed and purified as described before [39]. IC_{50} values for **5** were determined using a homogeneous fluorescence-based assay (see Table S1) [40]. Sirt1–Sirt3 were incubated with **5** at various concentrations [4 h, 37 °C, 10.5 μM ZMAL, 5% (v/v) DMSO, 500 μM NAD^+, 25 mM Tris, 137 mM NaCl, 2.7 mM KCl, 1 mM $MgCl_2$, pH 8.0, 60 μL]. Deacetylation was then stopped by addition of a trypsin solution [5.5 U/μL trypsin, 12 mM nicotinamide, 6.6% (v/v) DMSO, 50 mM Tris, 50 mM NaCl, pH 8.0, 60 μL], incubated (20 min, 37 °C) before fluorescence intensity was measured (λ_{Ex} = 390 nm, λ_{Em} = 460 nm; BMG Polarstar). Inhibition rates were determined in reference to a control with DMSO. Substrate conversion was adjusted to 10–30%. IC_{50} values were calculated with GraphPad Prism 5.0.

Crystallization and X-ray data collection

Co-crystallization of smHDAC8 together with **1a** was performed using hanging-drop vapor diffusion technique. The smHDAC8/**1a** complex was formed by incubating the smHDAC8 protein (2 mg/mL) with **1a** (5 mM resuspended in dimethylformamide) at 4 °C for 1 h. Diffraction-quality crystals were obtained at 17 °C after 3–4 days by mixing equal volumes of the smHDAC8/**1a** complexes with reservoir solution composed of 21% polyethylene glycol 3350 (Fluka) and 0.2 M Na^+/K^+ L-tartrate. Crystals used for X-ray data collection were briefly transferred in reservoir solution supplemented with 22% glycerol and flash-frozen in liquid nitrogen. Crystallographic data were collected at 100 K on in-house Rigaku MicroMax-007HF generator fitted with Osmic VariMax HF confocal optics and Saturn 944 CCD detector.

Structure determination, model building and refinement

Crystallographic data were processed and scaled using HKL2000 [41]. Since the crystals of the smHDAC8/**1a** complex belonged to the same space group (*P*1) and had the same unit cell as native smHDAC8 crystals [17], only rigid-body refinement was used to adapt to the slight differences in unit cell constants using Phenix [42].

The initial model was refined through several cycles of manual building using Coot [43] and automated refinement with Phenix [42] and Buster [44]. The final model was validated using tools provided in Coot [43]

and MolProbity [45]. The model has low *R*-factors and good refinement statistics (Table 2).

Computational methods

The recently solved crystal structures of *S. mansoni* HDAC8 with SAHA (PDB ID: 4BZ6 [17]) was used for the docking studies. For hHDAC8, several X-ray structures have been reported in complex with various inhibitors [46]. We took the crystal structure 2V5X.pdb [47] for the docking studies since it gave the best results in cross-docking of a large library of published and in-house HDAC8 inhibitors (data not shown). Structures were prepared with Schrödinger's Protein Preparation Wizard [48]. Hydrogen atoms were added and the hydrogen bond network was optimized subsequently. The protonation states were predicted using the PROPKA tool within the Schrödinger program at pH 7.0. Two conserved water molecules located near Zn^{2+} were considered during the protein preparation process. Four models with different hydration of the binding pocket were generated for each protein. They were subjected to restrained energy minimization using the force field OPLS2005 (RMSD of the atom displacement for terminating the minimization 0.3 Å).

Ligands were prepared in MOE [49] (version 2012.10; Chemical Computing Group, Montreal, Canada). Conformational search was performed using the Low Mode MD sampling with a minimum RMSD between the conformations of 0.5 Å to obtain realistic starting conformations for the flexible ligands.

Molecular docking was carried out on a Linux cluster using Glide (Schrödinger Inc, New York, USA) [48] in the standard precision mode. In addition, the docking program Gold 5.2 [50] was used. Finally, the docking complexes were rescored using several scoring functions (GlideSP, GoldScore, ChemScore, ASP, Chem-PLP). The best reproducibility of smHDAC8 and hHDAC8 inhibitor complexes was observed using Glide docking and rescoring with ASP score.

Antischistosomal effects of smHDAC8 inhibitors

A Puerto Rican strain of *S. mansoni* maintained in the laboratory using the intermediate snail host *Biomphalaria glabrata* and the golden hamster *Mesocricetus auratus* as definitive host was used. Cercariae were released from infected snails and harvested on ice as described previously [51], and schistosomula were obtained *in vitro* by mechanical transformation [52]. The effects of smHDAC8 inhibitors on the viability of schistosomula maintained in culture were assayed exactly as previously described [30]. Briefly, 2000 schistosomula were incubated at 37 °C in a humid atmosphere containing 5% CO_2 during 5 days in 6-well plates containing 2 mL of M199 medium (Invitrogen) kept at pH 7.4 with Hepes (10 mM) and supplemented with penicillin (50 U/mL), streptomycin (50 µg/mL), gentamycin (15 µg/mL) and rifampicin (60 µg/mL) and 10% fetal calf serum (Gibco) with different concentrations of inhibitors dissolved in DMSO. Culture medium was refreshed daily. Parasite mortality was assessed by eye each day using three criteria: absence of motility, tegument defects and granular appearance. A minimum of 300 larvae was observed for each condition, and the ratio of dead larvae to total larvae was calculated. Two different assays were performed for each condition and three independent biological replicates (different batches of schistosomula) were carried out.

To detect DNA strand breaks in inhibitor-treated schistosomula, we performed the TUNEL method with the *In Situ* Cell Death Detection Kit, TMR red (Roche), exactly as previously described [30]. Briefly, 2000 schistosomula were treated or not for 48 h with inhibitor as above. Culture medium was removed and the schistosomula were centrifuged (1000 rpm, 2 min), washed three times in phosphate-buffered saline and then fixed in 2% formaldehyde for 60 min. After a further wash in phosphate-buffered saline, permeabilization solution (0.1% Triton X-100, 0.1% sodium citrate) was added for 10 min on ice. Labeling of schistosomula with 4′,6-diamidino-2-phenylindole and TMR red dUTP was performed according to the manufacturer's instructions and TUNEL-positive parasites were observed by fluorescence using an AxioImager Z1-Apotome microscope (Zeiss).

Accession numbers

The atomic coordinates and structure factors of the smHDAC8/**1a** complex have been deposited in the Protein Data Bank under the accession code 4cqf. The PDB file of the complex is available as supplemental material to this paper.

Acknowledgments

This work and the authors of this manuscript received funding from the European Union's Seventh Framework Programme for research, technological development and demonstration under grant agreements nos. 241865 (SEtTReND) and 602080 (A-ParaDDisE). Research on dual HDAC/Sirt inhibitors in the Jung laboratory is funded by the Deutsche Forschungsgemeinschaft (Ju 295/10-2 within CRU201). The work of C.R., M.M., J.C., J.M.W., E.L., R.J.P. and J.L. was supported by institutional funds from the Centre National de la Recherche Scientifique, the Institut National de la Santé et de la Recherche Médicale, the Université de Strasbourg and the Université de Lille 2, the French Infrastructure for Integrated Structural Biology (ANR-10-INSB-05-01) and by Instruct (European Strategy Forum on Research

Infrastructures). We thank K. Schmidtkunz and J. Trolet for technical assistance.

Appendix A. Supplementary data

Supplementary data to this article can be found online at http://dx.doi.org/10.1016/j.jmb.2014.03.007.

Received 15 January 2014;
Received in revised form 13 March 2014;
Accepted 13 March 2014
Available online 20 March 2014

Keywords:
antiparasitic activity;
docking;
epigenetics;
thiol;
X-ray crystallography

Present address: D. A. Stolfa, Department of Pharmacy–Pharmaceutical Sciences, Università degli Studi di Bari Aldo Moro,via E. Orabona 4, 70125 Bari, Italy.

† D.A.S. and M.M. contributed equally to this work.

Abbreviations used:
smHDAC8, S. mansoni histone deacetylase 8; hHDAC8, human HDAC8; SAHA, suberoylanilide hydroxamic acid; HHA, hexanoylhydroxamate; SAA, suberanilic acid.

References

[1] WHO Mediacentre; Schistosomiasis (No. 115, January 2012). available at: http://www.who.int/mediacentre/factsheets/fs115/en/index.html.
[2] Wilson MS, Mentink-Kane MM, Pesce JT, Ramalingam TR, Thompson R, Wynn TA. Immunopathology of schistosomiasis. Immunol Cell Biol 2007;85:148–54.
[3] Doenhoff MJ, Kusel JR, Coles GC, Cioli D. Resistance of *Schistosoma mansoni* to praziquantel: is there a problem? Trans R Soc Trop Med Hyg 2002;96:465–9.
[4] Doenhoff MJ, Pica-Mattoccia L. Praziquantel for the treatment of schistosomiasis: its use for control in areas with endemic disease and prospects for drug resistance. Expert Rev Anti Infect Ther 2006;4:199–210.
[5] Messerli SM, Kasinathan RS, Morgan W, Spranger S, Greenberg RM. *Schistosoma mansoni* P-glycoprotein levels increase in response to praziquantel exposure and correlate with reduced praziquantel susceptibility. Mol Biochem Parasitol 2009;167:54–9.
[6] Zhou YP, Wu ZD, Yang LL, Sun X, You X, Yu XB, et al. Cloning, molecular characterization of a 13-kDa antigen from *Schistosoma japonicum*, Sj13, a putative salivary diagnosis candidate for *Schistosomiasis japonica*. Parasitol Res 2009;105:1435–44.
[7] Berriman M, Haas BJ, LoVerde PT, Wilson RA, Dillon GP, Cerqueira GC, et al. The genome of the blood fluke *Schistosoma mansoni*. Nature 2009;460:352–8.
[8] Protasio AV, Tsai IJ, Babbage A, Nichol S, Hunt M, Aslett MA, et al. A systematically improved high quality genome and transcriptome of the human blood fluke *Schistosoma mansoni*. PLoS Negl Trop Dis 2012;6:e1455.
[9] Young ND, Jex AR, Li B, Liu S, Yang L, Xiong Z, et al. Whole-genome sequence of *Schistosoma haematobium*. Nat Genet 2012;44:221–5.
[10] Jenuwein T, Allis CD. Translating the histone code. Science 2001;293:1074–80.
[11] Gardner KE, Allis CD, Strahl BD. Operating on chromatin, a colorful language where context matters. J Mol Biol 2011;409:36–46.
[12] Margueron R, Reinberg D. Chromatin structure and the inheritance of epigenetic information. Nat Rev Genet 2010;11:285–96.
[13] Thiagalingam S, Cheng KH, Lee HJ, Mineva N, Thiagalingam A, Ponte JF. Histone deacetylases: unique players in shaping the epigenetic histone code. Ann N Y Acad Sci 2003;983:84–100.
[14] Kouzarides T. Chromatin modifications and their function. Cell 2007;128:693–705.
[15] Dubois F, Caby S, Oger F, Cosseau C, Capron M, Grunau C, et al. Histone deacetylase inhibitors induce apoptosis, histone hyperacetylation and up-regulation of gene transcription in *Schistosoma mansoni*. Mol Biochem Parasitol 2009;168:7–15.
[16] Oger F, Dubois F, Caby S, Noel C, Cornette J, Bertin B, et al. The class I histone deacetylases of the platyhelminth parasite *Schistosoma mansoni*. Biochem Biophys Res Commun 2008;377:1079–84.
[17] Marek M, Kannan S, Hauser AT, Moraes Mourao M, Caby S, Cura V, et al. Structural basis for the inhibition of histone deacetylase 8 (HDAC8), a key epigenetic player in the blood fluke *Schistosoma mansoni*. PLoS Pathog 2013;9:e1003645.
[18] Jung M, Brosch G, Kolle D, Scherf H, Gerhauser C, Loidl P. Amide analogues of trichostatin A as inhibitors of histone deacetylase and inducers of terminal cell differentiation. J Med Chem 1999;42:4669–79.
[19] Scott GK, Marx C, Berger CE, Saunders LR, Verdin E, Schafer S, et al. Destabilization of ERBB2 transcripts by targeting 3′ untranslated region messenger RNA associated HuR and histone deacetylase-6. Mol Cancer Res 2008;6:1250–8.
[20] Fass DM, Reis SA, Ghosh B, Hennig KM, Joseph NF, Zhao WN, et al. Crebinostat: a novel cognitive enhancer that inhibits histone deacetylase activity and modulates chromatin-mediated neuroplasticity. Neuropharmacology 2013;64:81–96.
[21] Stowell JC, Huot RI, Van Voast L. The synthesis of *N*-hydroxy-*N*-phenyloctanediamide and its inhibitory effect on proliferation of AXC rat prostate cancer cells. J Med Chem 1995;38:1411–3.
[22] Suzuki T, Matsuura A, Kouketsu A, Nakagawa H, Miyata N. Identification of a potent non-hydroxamate histone deacetylase inhibitor by mechanism-based drug design. Bioorg Med Chem Lett 2005;15:331–5.
[23] Suzuki T, Nagano Y, Kouketsu A, Matsuura A, Maruyama S, Kurotaki M, et al. Novel inhibitors of human histone deacetylases: design, synthesis, enzyme inhibition, and cancer cell growth inhibition of SAHA-based non-hydroxamates. J Med Chem 2005;48:1019–32.
[24] Chen B, Petukhov PA, Jung M, Velena A, Eliseeva E, Dritschilo A, et al. Chemistry and biology of mercaptoacetamides as novel histone deacetylase inhibitors. Bioorg Med Chem Lett 2005;15:1389–92.
[25] Gu W, Nusinzon I, Smith RD, Horvath CM, Silverman RB. Carbonyl- and sulfur-containing analogs of suberoylanilide

hydroxamic acid: potent inhibition of histone deacetylases. Bioorg Med Chem 2006;14:3320–9.
[26] Ueda H, Nakajima H, Hori Y, Fujita T, Nishimura M, Goto T, et al. FR901228, a novel antitumor bicyclic depsipeptide produced by *Chromobacterium violaceum* No. 968. I. Taxonomy, fermentation, isolation, physico-chemical and biological properties, and antitumor activity. J Antibiot (Tokyo) 1994;47:301–10.
[27] VanderMolen KM, McCulloch W, Pearce CJ, Oberlies NH. Romidepsin (Istodax, NSC 630176, FR901228, FK228, depsipeptide): a natural product recently approved for cutaneous T-cell lymphoma. J Antibiot (Tokyo) 2011;64:525–31.
[28] Kijima M, Yoshida M, Sugita K, Horinouchi S, Beppu T. Trapoxin, an antitumor cyclic tetrapeptide, is an irreversible inhibitor of mammalian histone deacetylase. J Biol Chem 1993; 268:22429–35.
[29] Uesato S, Kitagawa M, Nagaoka Y, Maeda T, Kuwajima H, Yamori T. Novel histone deacetylase inhibitors: *N*-hydroxycarboxamides possessing a terminal bicyclic aryl group. Bioorg Med Chem Lett 2002;12:1347–9.
[30] Lancelot J, Caby S, Dubois-Abdesselem F, Vanderstraete M, Trolet J, Oliveira G, et al. *Schistosoma mansoni* sirtuins: characterization and potential as chemotherapeutic targets. PLoS Negl Trop Dis 2013;7:e2428.
[31] Trapp J, Jochum A, Meier R, Saunders L, Marshall B, Kunick C, et al. Adenosine mimetics as inhibitors of NAD^+-dependent histone deacetylases, from kinase to sirtuin inhibition. J Med Chem 2006;49:7307–16.
[32] Whitehead L, Dobler MR, Radetich B, Zhu Y, Atadja PW, Claiborne T, et al. Human HDAC isoform selectivity achieved via exploitation of the acetate release channel with structurally unique small molecule inhibitors. Bioorg Med Chem 2011;19:4626–34.
[33] Balasubramanian S, Ramos J, Luo W, Sirisawad M, Verner E, Buggy JJ. A novel histone deacetylase 8 (HDAC8)-specific inhibitor PCI-34051 induces apoptosis in T-cell lymphomas. Leukemia 2008;22:1026–34.
[34] Cole KE, Dowling DP, Boone MA, Phillips AJ, Christianson DW. Structural basis of the antiproliferative activity of largazole, a depsipeptide inhibitor of the histone deacetylases. J Am Chem Soc 2011;133:12474–7.
[35] Sung YM, Lee T, Yoon H, DiBattista AM, Song JM, Sohn Y, et al. Mercaptoacetamide-based class II HDAC inhibitor lowers Abeta levels and improves learning and memory in a mouse model of Alzheimer's disease. Exp Neurol 2013;239:192–201.
[36] Kalin JH, Zhang H, Gaudrel-Grosay S, Vistoli G, Kozikowski AP. Chiral mercaptoacetamides display enantioselective inhibition of histone deacetylase 6 and exhibit neuroprotection in cortical neuron models of oxidative stress. ChemMedChem 2012;7:425–39.
[37] Kozikowski AP, Chen Y, Gaysin A, Chen B, D'Annibale MA, Suto CM, et al. Functional differences in epigenetic modulators-superiority of mercaptoacetamide-based histone deacetylase inhibitors relative to hydroxamates in cortical neuron neuroprotection studies. J Med Chem 2007;50:3054–61.
[38] Diebold ML, Fribourg S, Koch M, Metzger T, Romier C. Deciphering correct strategies for multiprotein complex assembly by co-expression: application to complexes as large as the histone octamer. J Struct Biol 2011;175:178–88.
[39] Maurer B, Rumpf T, Scharfe M, Stolfa DA, Schmitt ML, He WJ, et al. Inhibitors of the NAD(+)-dependent protein desuccinylase and demalonylase Sirt5. ACS Med Chem Lett 2012;3: 1050–3.
[40] Heltweg B, Trapp J, Jung M. *In vitro* assays for the determination of histone deacetylase activity. Methods 2005;36:332–7.
[41] Otwinowski Z, Minor W. Processing of X-ray diffraction data collected in oscillation mode. Methods Enzymol 1997;276: 307–26.
[42] Adams PD, Afonine PV, Bunkoczi G, Chen VB, Davis IW, Echols N, et al. PHENIX: a comprehensive Python-based system for macromolecular structure solution. Acta Crystallogr Sect D Biol Crystallogr 2010;66:213–21.
[43] Emsley P, Cowtan K. Coot: model-building tools for molecular graphics. Acta Crystallogr Sect D Biol Crystallogr 2004;60: 2126–32.
[44] Blanc E, Roversi P, Vonrhein C, Flensburg C, Lea SM, Bricogne G. Refinement of severely incomplete structures with maximum likelihood in BUSTER-TNT. Acta Crystallogr Sect D Biol Crystallogr 2004;60:2210–21.
[45] Chen VB, Arendall WB, Headd JJ, Keedy DA, Immormino RM, Kapral GJ, et al. MolProbity: all-atom structure validation for macromolecular crystallography. Acta Crystallogr Sect D Biol Crystallogr 2010;66:12–21.
[46] The Research Collaboratory for Structural Bioinformatics Protein Data Bank. http://www.rcsb.org/pdb/.
[47] Vannini A, Volpari C, Gallinari P, Jones P, Mattu M, Carfi A, et al. Substrate binding to histone deacetylases as shown by the crystal structure of the HDAC8-substrate complex. EMBO Rep 2007;8:879–84.
[48] Suite 2012: Maestro version 9.3, Protein Preparation Wizard, Epik version 2.3, Glide version 5.8. New York, NY: Schrödinger, LLC; 2012.
[49] Molecular Operating Environment (MOE), 2012.10. Montreal, QC, Canada: Chemical Computing Group Inc.; 2012.
[50] Jones G, Willett P, Glen RC, Leach AR, Taylor R. Development and validation of a genetic algorithm for flexible docking. J Mol Biol 1997;267:727–48.
[51] Bertin B, Oger F, Cornette J, Caby S, Noel C, Capron M, et al. *Schistosoma mansoni* CBP/p300 has a conserved domain structure and interacts functionally with the nuclear receptor SmFtz-F1. Mol Biochem Parasitol 2006;146:180–91.
[52] Ramalho-Pinto FJ, Gazzinelli G, Howells RE, Mota-Santos TA, Figueiredo EA, Pellegrino J. *Schistosoma mansoni*: defined system for stepwise transformation of cercaria to schistosomule *in vitro*. Exp Parasitol 1974;36:360–72.